BEYOND THE DAMPING TAIL:
CROSS-CORRELATING THE KINETIC SUNYAEV-ZEL'DOVICH EFFECT WITH COSMIC SHEAR

OLIVIER DORÉ, JOSEPH F. HENNAWI, & DAVID N. SPERGEL
Department of Astrophysical Sciences, Peyton Hall, Ivy Lane, Princeton University, NJ-08544, USA
email: olivier@astro.princeton.edu, jhennawi@astro.princeton.edu, dns@astro.princeton.edu
Draft version October 28, 2018

ABSTRACT

Secondary anisotropies of the CMB have the potential to reveal intricate details about the history of our universe between the present and recombination epochs. However, because the CMB we observe is the projected sum of a multitude of effects, the interpretation of small scale anisotropies by future high resolution experiments will be marred by uncertainty and speculation without the handles provided by other observations. The recent controversy over the *excess* small scale anisotropy detected by CBI and the BIMA array is a foretaste of potential challenges that will be faced when interpreting future experiments. In this paper we show that cross correlating the CMB with an overlapping weak lensing survey will isolate the elusive kinetic Sunyaev-Zel'dovich Effect from secondary anisotropies generated at higher redshifts. We show that if upcoming high angular resolution CMB experiments, like PLANCK/ACT/SPT, cover the same area of sky as current and future weak lensing surveys, like CFTHLS/SNAP/LSST, the cross correlation of cosmic shear with the kSZ effect will be detected with high signal to noise ratio, increasing the potential science accessible to both sets of surveys. For example, if ACT and a CFHTLS like survey were to overlap this cross-correlation would be detected with a total signal to noise ratio greater than 220, reaching 1.8 per individual multipole around $l \sim 5000$. Furthermore, this cross-correlation probes the three point coupling between the underlying dark matter and the *momentum* of the ionized baryons in the densest regions of the universe at intermediate redshifts. Similar to the tSZ power spectrum, its strength is extremely sensitive to the power spectrum normalization parameter, σ_8, scaling roughly as σ_8^7. It provides an effective mechanism to isolate any component of anisotropy due to patchy reionization and rule out primordial small scale anisotropy.

Subject headings: cosmology: theory – cosmology: observation – cosmology: weak lensing – cosmology: peculiar velocities – galaxies: formation – galaxies: evolution

1. INTRODUCTION

The Wilkinson Microwave Anisotropy Probe (WMAP) [1] has ushered in an era of unprecedented accuracy for measurements of the cosmic microwave background (CMB) anisotropy. Future high angular resolution experiments like PLANCK[2], the Atacama Cosmology Telescope (ACT)[3], and the South Pole Telescope (SPT)[4] will measure arc-minute scale ($\ell \gtrsim 1000$) anisotropies at the μK level. The primary anisotropies generated at the epoch of recombination and measured by WMAP (Spergel *et al.* 2003) involve calculations in linear perturbation theory and are on sound theoretical footing (see however Bean *et al.* 2003, and references therein for a discussion of alternative models). However, secondary anisotropies, caused by highly nonlinear structures and involving complicated dissipative baryonic physics, are still a subject of theoretical speculation

In considering secondary anisotropies, a practical distinction must be made between anisotropies that have a CMB-like thermal spectrum, and the anisotropies with a non thermal frequency dependence, most notably the thermal Sunyaev-Zel'dovich effect (tSZ) (Sunyaev & Zel'dovich 1980). Although challenging and imperfect, it should be possible to isolate these ther-

mal contributions from a temperature map using the specific frequency and spatial dependence of the latter (Bouchet & Gispert 1999; Tegmark & Efstathiou 1996). After these non-thermal components have been removed, the dominant sources of secondary anisotropies are expected to be — from degree to arc-minute scales — the Rees-Sciama effect (RS)(Rees & Sciama 1968), the weak gravitational lensing of the CMB itself, the kinetic Sunyaev-Zel'dovich (kSZ) effect and possibly patchy reionization (Sunyaev & Zel'dovich 1980 and Santos *et al.* 2003 for recent references). Given a "frequency cleaned" temperature map containing the sum of these secondary effects, it would be desirable to study each component individually in order to evaluate their consistency with theoretical predictions. If the CMB temperature were studied in conjunction with another low redshift tracer of the cosmological density field, the presence or absence of correlations between the two might provide a mechanism to isolate the various components.

The recent detection of *excess* small scale anisotropy is a nice illustration of the preceding discussion and provides a foretaste of the potential challenges that will be faced when interpreting the secondary anisotropies detected by future experiments. At angular scales of a several arc-minutes at multipoles beyond the damping tail ($\ell \gtrsim 2000$), the CBI experiment (Mason *et al.* 2003) and the BIMA array (Dawson *et al.* 2002) have both detected temperature anisotropy at a level of $\sim 500\mu K^2$

with significance of $\gtrsim 3\sigma$. Although a natural interpretation of this excess power is tSZ, the strength of the signal requires that the power spectrum normalization parameter take on a value $\sigma_8 \approx 1$ in the upper range allowed by current CMB and Large Scale Structure data (Bond *et al.* 2003; Komatsu & Seljak 2002). Furthermore, the required value is likely even higher because the measured anisotropy, if thermal SZ, was likely diluted by radio point source subtraction (Holder 2002). Both the CBI and BIMA experiments observe at low frequencies ~ 30 GHz well into the Rayleigh-Jeans region of the thermal SZ frequency spectrum, so at present the non-thermal frequency signature of the tSZ effect cannot be exploited to determine the nature of this excess. This has led to considerable speculation about other sources of arc-minute scale anisotropy possibly arising from the epoch of reionization or the early universe. While the kSZ effect and patchy reionization are not expected to produce small scale anisotropies at the level detected, it has been suggested that the excess power is due to SZ fluctuations from high-z $\gtrsim 10$ star formation (Oh *et al.* 2003), primordial voids created by bubble nucleation during the inflationary epoch (Griffiths, Kunz, & Silk 2003), or broken scale invariance in the primordial power spectrum produced by inflation (Cooray & Melchiorri 2002). Cross correlating the CMB temperature maps measured by CBI and BIMA with a low redshift tracer of the density field would provide a mechanism to determine whether the small scale excess was generated in the local universe. The detection of a correlation with galaxies would favor tSZ or radio source contamination rather than the more speculative alternatives.

Cosmologists will likely face similar uncertainties in the future for experiments that will have the frequency coverage required to produce frequency cleaned temperature maps that effectively remove the tSZ. Cross correlation with a local density tracer could provide the most effective means to determine the source of the anisotropy. For example, the patchy reionization signal or some exotic form of small scale anisotropy generated by inflation will not correlate with low redshift density tracers; whereas, the kinetic SZ effect should correlate strongly, which brings us to the subject of this work. Weak gravitational lensing, or the coherent distortion of images of faint background galaxies by the foreground matter distribution (see Van Waerbeke & Mellier 2003, for a recent review), is a tracer of the local density field, with the added advantage that it probes the dark matter directly, foregoing the complications caused by issues of bias in galaxy surveys. In this paper we compute the correlation between weak gravitational lensing and the kinetic Sunyaev-Zel'dovich effect and evaluate the prospects of future experiments to measure it.

Although the cross-correlations between secondary anisotropies and weak gravitational lensing of the CMB itself, has been considered previously (Spergel & Goldberg 1999, Goldberg & Spergel 1999, Cooray & Hu 2000, Takada & Sugyama 2002, Verde & Spergel 2002), the potential correlation signals between the CMB and galaxy weak lensing, or "cosmic shear" has been somewhat neglected. In particular, we focus on previously unexplored small angular scales beyond the "damping tail," which will be probed by the aforementioned future experiments.

The overlap of angular scales between secondary anisotropies of the CMB and cosmic shear is illustrated in figure 1. Error bars are shown for current and future CMB experiments and weak lensing surveys. Theoretical estimates for primary and secondary anisotropies are shown in the left panel, and predictions for the power spectrum of the weak lensing convergence field is shown at right. Seljak, Burwell, & Pen (2001) calculated the correlation between cosmic shear and the thermal Sunyaev-Zel'dovich effect (tSZ). Once the tSZ signal is removed by frequency cleaning, the Rees-Sciama effect, CMB lensing, kinetic SZ, and possibly patchy reionization remain. Hu (2002) considered the correlation between cosmic shear and both the linear ISW effect and CMB lensing. As is visible in the figure, the nonlinear correction to the ISW effect, known as the Rees-Sciama effect is important on small scales $\ell \gtrsim 300$, and we compute the correlation between cosmic shear and the Rees-Sciama effect in a companion paper (Doré *et al.* 2003). For $\ell \gtrsim 3000$, the kinetic SZ spectrum intersects the lensed CMB damping tail, and will likely dominate the anisotropy spectrum, (we have plotted the maximal patchy reionization signal for illustration).

Below we calculate the fully nonlinear cross correlation between cosmic shear and the kinetic SZ effect. This calculation is complicated by the fact that the kSZ effect is proportional to the velocity of the ionized baryons, $\Delta T/T \sim \mathbf{v}$; hence, any two point correlation with a density tracer will be negligible for an isotropic velocity field. This is simply the statement that the over-density field δ is just as likely to correlate with a cluster moving toward us as one moving away from us, and thus the average correlation vanishes. In fact, the isotropy of the velocity field guarantees that any statistic of odd powers of the velocity field is highly suppressed relative to even statistics (Monin & Yaglom 1971, Scannapieco 2000, Castro 2003). Thus, we must work with a three point statistic – two kSZ points and one weak lensing — and we consider a "collapsed" configuration. That is we calculate the two point function of weak lensing and the filtered CMB temperature squared, which condenses three point information into an easily measurable power spectrum.

We model the observables in § 2 and calculate the angular auto power spectra of weak lensing and kinetic SZ which are shown fig. 1. Special attention is paid to the approximations and analytical techniques used to calculate these auto power spectra in the fully nonlinear regime. The cross-correlation signals are calculated in § 3. In § 4 we attempt to qualitatively understand why cosmic shear is correlated with the square of kinetic SZ, and the dependence of the correlation signal on the power spectrum normalization is explored in § 5. A signal to noise ratio analysis is performed in § 6, to quantify the prospect for detecting this correlation for current and future experiments. We discuss our results, discuss limitations, and conclude in § 7.

Throughout this paper we consider only flat cosmologies. As our fiducial model we choose the best fit WMAP (only) model of Spergel *et al.* (2003), with $\Omega_m = 0.270$, $\Omega_\Lambda = 0.73$, $h = 0.72$, $n_s = 0.97$, $\sigma_8 = 0.84$ and $\tau = 0.17$.

2. MODELING THE OBSERVABLES

We define in this section the needed general equations before introducing the effect that will be discussed throughout this paper. We calculate their angular auto
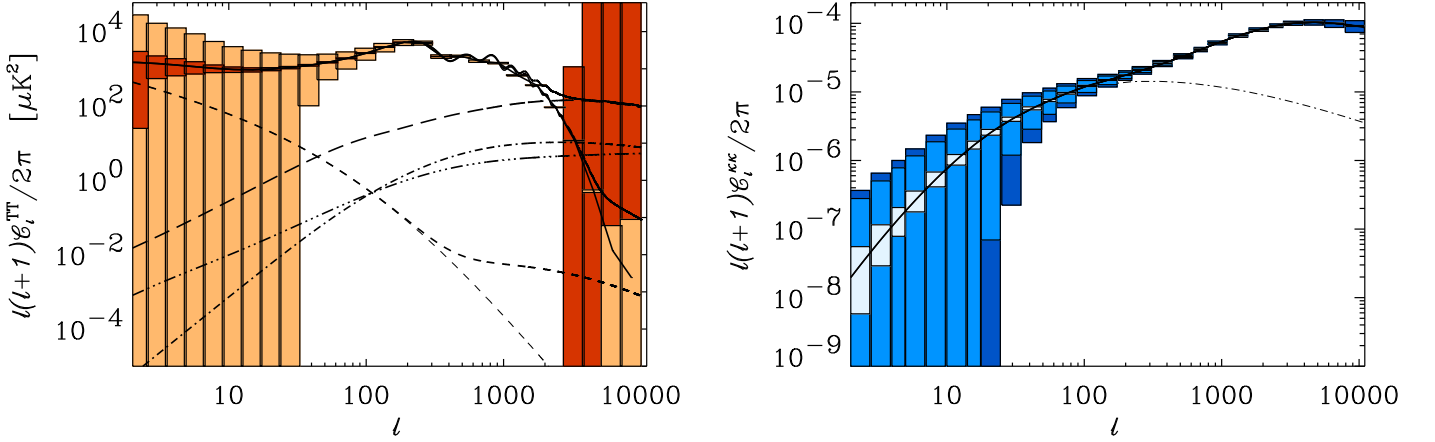
FIG. 1.— *Left:* Expected signal and errors for the coming PLANCK and ACT CMB experiments (see §6 for precise assumptions). The Bordeaux wine color refers to PLANCK whereas the cream one refers to ACT. The cosmic variance is computed assuming the primordial power spectrum only, which is obviously an lower limit. The thick solid line denotes the primordial CMB signal with (up) or without (down) the lensing contribution. The thick short-dashed line denotes the ISW effect (low ℓ) and the non-linear RS effect (high ℓ). Note the angular transition between both. The thick long-dashed line denotes the expected thermal SZ contribution according to (Komatsu & Seljak 2002). The thick double-dot-dashed line corresponding to the expected kSZ, whereas the dot-dashed line corresponds to a possible component induced by patchy-reionisation (note that the overall amplitude is rather model-dependent and that we here assume the strongest signal (Santos *et al.* 2003)). The thin solid line denotes the sum of all those contributions. *Right:* Expected signal and error for the coming CFHTLS, SNAP and LSST experiments (see §6 for precise assumptions). We consider here only shot noise due to intrinsic ellipticities and cosmic variance, and assume that both dominates over systematics at any scale. We assume for this illustration only that this 3 surveys measure the same convergence power spectrum. We thus neglect the effects of the different sources populations. From darker to lighter, the 3 depicted error boxes correspond to CFHTLS, SNAP and LSST.

power spectra and sketches their cross-correlation. The calculations in this section are complicated by the fact that the three dimensional fields whose power spectra and bispectra we desire are highly nonlinear. Special attention is paid to the approximations and analytical techniques used to calculate these nonlinear power spectra.

2.1. *Angular Power Spectra in the Flat Sky Approximation*

We will be interested in the angular power spectra of fields on the sky $X(\hat{\mathbf{n}})$ which are weighted line-of-sight projections of three dimensional fields which we denote δ_X,

$$X(\hat{\mathbf{n}}) = f^X \star \left(\int d\eta \, W^X(\eta) \delta_X(\eta\hat{\mathbf{n}}, \eta) \right) \qquad (1)$$

where $W^X(\eta)$ is the weight function for the field X and f^X is a real space isotropic filter with which we convolve this field. We define the conformal "look back" time as $\eta = \tau_0 - \tau$, which can also be interpreted as the comoving distance. Here τ is the conformal time $d\tau = (1/a)$, τ_0, which can also be interpreted as the comoving distance from the observer. Here and throughout we set $c = 1$

For small sections of the sky or high multipole moments, it is a good approximation to treat the sky as flat. In this flat-sky approximation, the Fourier moments of this field on the sky are

$$\tilde{X}(\boldsymbol{\ell}) = \int d^2\mathbf{n} \, X(\hat{\mathbf{n}}) e^{-i\boldsymbol{\ell}\cdot\hat{\mathbf{n}}} \qquad (2)$$

Combining with eq. (1) gives

$$\tilde{X}(\boldsymbol{\ell}) = f^X(\ell) \int \frac{d\eta}{\eta^2} W^X(\eta) \int \frac{dk_z}{2\pi} \tilde{\delta}(\mathbf{k}_\perp = \boldsymbol{\ell}/\eta, k_z) e^{ik_z\eta}, \qquad (3)$$

where $f^X(\ell)$ is the Fourier transform of f^X.

As in the all sky case, the cross correlation (or auto power spectrum) for any two fields, X and Z is defined by

$$\langle \tilde{X}^*(\boldsymbol{\ell})\tilde{Z}(\boldsymbol{\ell})\rangle = (2\pi)^2\delta_D(\boldsymbol{\ell} + \boldsymbol{\ell}')C^{XZ}(\ell), \qquad (4)$$

and similarly the power spectrum between two three dimensional fields δ_X and δ_Z is

$$\langle \tilde{\delta}_X(\mathbf{k}, \eta)\tilde{\delta}_Z(\mathbf{k}, \eta)\rangle = (2\pi)^3\delta_D(\mathbf{k} + \mathbf{k}')P_{XZ}(k, \eta), \qquad (5)$$

Where δ_D is the Dirac delta function.

For the relationship between these flat-sky Fourier modes and the spherical harmonic coefficients $X_{\ell m}$ and a proof of the correspondence between the angular power spectrum C_ℓ^{XZ} and $C^{XZ}(\ell)$, see e.g. White *et al.* (1999) or Appendix C of Hu (2000).

Combining eqs. (3), (4), and (5), the correlation between X and Z is

$$\langle \tilde{X}^*(\boldsymbol{\ell})\tilde{Z}(\boldsymbol{\ell}')\rangle = (2\pi)^2 f^X(\ell)f^Z(\ell) \int d\eta \frac{W^X(\eta)}{\eta^2}$$
$$\times \int d\eta' \frac{W^Z(\eta')}{\eta'^2} \int \frac{dk_z}{2\pi} e^{ik_z(\eta-\eta')}$$
$$\delta_D(\boldsymbol{\ell}/\eta + \boldsymbol{\ell}'/\eta')P_{XZ}(\sqrt{(\boldsymbol{\ell}/\eta)^2 + k_z^2}) (6)$$

Provided that the window functions $W(\eta)$ are slowly varying, $k \gg \dot{W}^X/W^X$, we can work in the Limber approximation (Kaiser 1992), allowing us to neglect radial

modes relative to perpendicular modes, $k_z \ll \ell/\eta$, and we arrive at

$$\Delta_{XZ}^2(\ell) = \frac{\pi}{\ell} f^X(\ell) f^Z(\ell) \int d\ln\eta \; \eta^2 W^X(\eta) W^Z(\eta)$$
$$\times \Delta_{XZ}^2(k = \ell/\eta, \eta) \qquad (7)$$

where the we have introduced the dimensionless angular power spectrum $\Delta_{XZ}^2(\ell) = \frac{\ell^2}{2\pi} C_\ell^{XZ}$, and the dimensionless 3-d power spectrum $\Delta_{XZ}^2(k,\eta) = k^3/2\pi^2 P_{XZ}(k,\eta)$. In the following section, we list the relevant window functions and discuss the phenomenological techniques used to calculate the three dimensional power spectra in the fully nonlinear regime. Note that until § 6, we set $f^X(\ell) = 1$.

2.2. *Weak Gravitational Lensing*

The distortion of background source galaxies by the foreground matter distribution is completely described by the convergence field $\kappa(\hat{\mathbf{n}})$ in the weak lensing approximation, which is a weighted projection of the density field along the line of sight

$$\kappa(\hat{\mathbf{n}}) = \int_0^{\tau_0} d\eta W^\kappa(\eta) \; \delta(\eta\hat{\mathbf{n}}, \eta), \qquad (8)$$

where the kernel is given by (for a flat cosmology)

$$W^\kappa(\eta) = \frac{3\Omega_{m0}H_0^2\eta}{2a} \int_\eta^{\tau_0} d\eta' \frac{\eta'-\eta}{\eta'} S(\eta'), \qquad (9)$$

and $S(\eta')$ describes the normalized radial distribution of sources

$$S(\eta) = p_z(z)\frac{d\eta}{dz}, \qquad (10)$$

with $p_z(z)$ being the normalized source redshift distribution $\int dz p_z(z) = 1$, which in principle can be measured from the weak lensing survey. For definiteness, we use

$$p_z(z) = \frac{1}{2z_0^3} z^2 e^{-z/z0}. \qquad (11)$$

This redshift distribution peaks at $2z_0$, has mean redshift $\langle z \rangle = 3z_0$, and has been used in previous studies of cosmic shear (Wittman et al. 2000). The values of z_0 that we use to represent current and future surveys, along with the other specifications are listed in table 2.

In order to evaluate the weak lensing power spectrum we need an expression for the fully nonlinear power spectrum of the over-density field $P_{\delta\delta}(k)$. Fitting formula for the nonlinear power spectrum have been studied extensively (Hamilton et al. 1991; Ma 1998; Peacock & Dodds 1996; Smith *et al.* 2003). We use the scaling formula of Smith *et al.* (2003) for the nonlinear power spectrum, which is accurate at better than the 10% level.

The angular power spectrum C_ℓ^κ of the *cosmic shear* is shown in fig. 1. Error bars are shown for current and future surveys which will have different source redshift distributions, although for illustration, we show only the case $z_0 = 0.5$.

2.3. *The kinetic SZ effect*

CMB photons diffusing to us from the surface of last scattering are up-scattered by the electron plasma bound in the gravitational potentials of dark matter halos. The motion and density variations of those scatterers will imprint a specific thermal temperature fluctuation pattern on the CMB, $\Theta^{\mathrm{kSZ}} = \Delta T_{kSZ}/T_0$, both because of the Doppler effect and of variations in opacity (Sunyaev & Zel'dovich 1980),

$$\Theta^{\mathrm{kSZ}}(\hat{\mathbf{n}}) = \int_0^{\tau_0} d\eta \; g(\eta) \, \hat{\mathbf{n}} \cdot \mathbf{p}(\hat{\mathbf{n}}\eta, \eta) \qquad (12)$$

where we have introduced the momentum density

$$\mathbf{p}(\hat{\mathbf{n}}\eta, \eta) = (1 + \delta(\hat{\mathbf{n}}\eta, \eta))\mathbf{v}(\hat{\mathbf{n}}\eta, \eta) \qquad (13)$$

and the visibility function, g. The latter can be expressed in terms of the Thomson optical depth, $\tau(\eta) = \int_0^\eta \dot{\tau}(\eta)d\eta$, where $\dot{\tau}(\eta) = a(\eta)n_e x_e \sigma_T$ with σ_T the Thomson scattering cross section, n_e the electron density and x_e the ionization fraction. Thus

$$g(\eta) = \frac{d\tau}{d\eta}e^{-\tau} = x_e \tau_H (1+z)^2 e^{-\tau}, \qquad (14)$$

where

$$\tau_H = 0.0691 (1 - Y_p) \Omega_b h, \qquad (15)$$

is the Thomson scattering optical depth to the Hubble distance today, assuming full hydrogen ionization, and Y_p is the primordial helium fraction. We assume further that reionization occurs instantaneously, *i.e.* $x_e = 1$ at all times after the reionization epoch, z_{ri}. Then we have (Griffiths, Barbosa, & Liddle 1999)

$$\tau(z_{ri}) = \frac{2}{3}\frac{\tau_H}{\Omega_m}\left[\sqrt{1 - \Omega_m + \Omega_m (1+z_{ri})^3} - 1\right] \qquad (16)$$

for a flat universe.

As was first pointed out by Kaiser (1984), cancellation of successive peaks and troughs for small wavelength modes prevents a significant kinetic SZ effect from contributing to the CMB anisotropy at linear order. This can be understood in the context of the 'Limber' (Kaiser 1992) or 'weak coupling' (Hu & White 1996) approximations. They dictate that only modes with wave-vectors perpendicular to the line of sight contribute to the projection of a given random field, because uncorrelated radial waves cancel in the line of sight projection. Gravity generates potential velocity flows, so that radial velocities have no wave-vector component perpendicular, in Fourier space, to the line of sight; consequently, the linear Doppler effect $\mathbf{p} \sim \mathbf{v}$ vanishes.

Ostriker & Vishniac (1986) showed that the same will be not be true for density modulated velocity flows, $\mathbf{p} \sim \delta\mathbf{v}$, which can have a non-vanishing curl. Thus wave-vectors perpendicular to the line of sight generate fluctuations parallel to the line of sight. At second order in perturbation theory, this is known as the Ostriker-Vishniac effect (Dodelson & Jubas 1995; Hu & White 1996; Ostriker & Vishniac 1986; Vishniac 1987); whereas, the full nonlinear signal is referred to as the kinetic-SZ (kSZ) effect. This full non-linear contribution has been studied in detail both analytically (Hu 2000; Ma & Fry 2001; Zhang *et al.* 2003) and numerically (da Silva *et al.* 2001; Gnedin & Jaffe 2001; Springel *et al.* 2001; Zhang *et al.* 2003).

Although the amplitude of the expected signal is uncertain, the maximal signal can be calculated if we assume that the electrons trace the dark matter exactly.

Then we can write for the power spectrum of the radial momentum component $p_{\hat{\mathbf{n}}}$ (Hu 2000; Ma & Fry 2000)

$$P_{p_{\hat{\mathbf{n}}}p_{\hat{\mathbf{n}}}}(k) \approx \frac{1}{2}P_{\mathbf{p}_{\perp}\mathbf{p}_{\perp}}(k) \approx \frac{1}{3}v_{\mathrm{rms}}^2 P_{\delta\delta}^{\mathrm{nl}}. \qquad (17)$$

where $P_{\mathbf{p}_{\perp}\mathbf{p}_{\perp}}$ is the power spectrum of the *vortical* component of the momentum field $\mathbf{p}_{\perp}$. This assumes the dominant contribution to the power spectrum of the radial momentum comes from nonlinear densities coupling to linear bulk velocity flows (Hu 2000; Ma & Fry 2001; though see also Zhang *et al.* 2003). The right panel of fig. 3 shows the 3-d auto power spectrum $P_{p_{\hat{\mathbf{n}}}p_{\hat{\mathbf{n}}}}$ at $z = 0.5$. The projection of this power spectrum with eq. (7) gives the angular kSZ power spectrum, which is shown in fig. 1.

3. THE KINETIC SZ WEAK LENSING CORRELATION

In this section we compute the correlation between the kinetic SZ effect and weak gravitational lensing. This calculation is complicated by the fact that the simple two point correlation $\langle\kappa\Theta\rangle$, will vanish because $\Theta^{\mathrm{kSZ}} \sim \mathbf{v}$, and the velocity field is isotropic. This is just the statement that the over-density field δ is just as likely to correlate with a cluster moving toward us as one moving away from us, and the average correlation vanishes. The isotropy of the velocity field guarantees that statistics of odd powers of the velocity field are highly suppressed relative to even statistics (Monin & Yaglom 1971, Scannapieco 2000, Castro 2003).

Thus a non-vanishing correlation requires that we work with a three point statistic: two kSZ points, so that our statistic is even in the velocity, and one point weak lensing. We consider the simplest case of a "collapsed" three point function — the cross correlation between the kappa field and the square of the kSZ, $\langle\kappa\Theta^2\rangle$ — which condenses three point information into an easily measurable angular power spectrum.

Squaring the temperature field couples multipoles at all scales, and in particular, power from multipoles outside the range where the kSZ is dominant, will swamp the signal. To prevent our quadratic temperature statistic from being polluted by the beam and primary anisotropies, we must filter the temperature before squaring

$$\tilde{\Theta}_f(\boldsymbol{\ell}) = f(\boldsymbol{\ell})\tilde{\Theta}(\boldsymbol{\ell}) \qquad (18)$$

This simple convolution before squaring is a special case of a more general class of filters for quadratic temperature statistics studied by Hu (2002).

3.1. *Limber approximation for the bispectrum*

In the flat sky approximation, the square of the filtered temperature fluctuation can be written as a convolution in (2D) Fourier space,

$$\tilde{\Theta}_f^2(\boldsymbol{\ell}') = \int \frac{d^2\boldsymbol{\ell}''}{(2\pi)^2}\tilde{\Theta}_f(\boldsymbol{\ell}'')\tilde{\Theta}_f(\boldsymbol{\ell}'-\boldsymbol{\ell}''), \qquad (19)$$

and the weak lensing kinetic SZ squared correlation is

$$\langle\tilde{\kappa}(\boldsymbol{\ell})\tilde{\Theta}_f^2(\boldsymbol{\ell}')\rangle = \int \frac{d^2\boldsymbol{\ell}''}{(2\pi)^2}\langle\tilde{\kappa}(\boldsymbol{\ell})\tilde{\Theta}_f(\boldsymbol{\ell}'')\tilde{\Theta}_f(\boldsymbol{\ell}'-\boldsymbol{\ell}'')\rangle \quad (20)$$

with

$$\langle\tilde{\kappa}(\boldsymbol{\ell})\tilde{\Theta}_f(\boldsymbol{\ell}'')\tilde{\Theta}_f(\boldsymbol{\ell}'-\boldsymbol{\ell}'')\rangle = (2\pi)^2 f(\ell)f(|\boldsymbol{\ell}'-\boldsymbol{\ell}''|)$$

$$\times \int d\eta \frac{W^{\kappa}(\eta)}{\eta^2} \int d\eta' \frac{g(\eta')}{\eta'^2} \int d\eta'' \frac{g(\eta'')}{\eta''^2}$$

$$\times \int \frac{dk_z}{2\pi}e^{ik_z(\eta-\eta')} \int \frac{dk_z'}{2\pi}e^{ik_z''(\eta''-\eta')} \qquad (21)$$

$$\times \delta_D(\boldsymbol{\ell}/\eta + \boldsymbol{\ell}''/\eta'' + (\boldsymbol{\ell}'-\boldsymbol{\ell}'')/\eta')$$

$$\times B_{\delta p_{\hat{\mathbf{n}}}p_{\hat{\mathbf{n}}}}(\boldsymbol{\ell}/\eta + \mathbf{k}_z, \boldsymbol{\ell}''/\eta'' + \mathbf{k}_z'', (\boldsymbol{\ell}'-\boldsymbol{\ell}'')/\eta' - (\mathbf{k}_z + \mathbf{k}_z'')),$$

where we have introduced the *hybrid* bispectrum

$$\langle\tilde{\delta}(\mathbf{k}_1)\tilde{p}_{\hat{\mathbf{n}}}(\mathbf{k}_2)\tilde{p}_{\hat{\mathbf{n}}}(\mathbf{k}_3)\rangle =$$
$$(2\pi)^3 B_{\delta p_{\hat{\mathbf{n}}}p_{\hat{\mathbf{n}}}}(\mathbf{k}_1, \mathbf{k}_2, \mathbf{k}_3)\,\delta_D(\mathbf{k}_1 + \mathbf{k}_2 + \mathbf{k}_3). \quad (22)$$

The expression in eq. (22) can be simplified in the Limber approximation for the bispectrum (Buchalter *et al.* 2000), valid for the small angles considered here. We can again ignore radial modes $k_z \ll \ell/\eta$, giving

$$\langle\tilde{\kappa}(\boldsymbol{\ell})\tilde{\Theta}_f(\boldsymbol{\ell}'')\tilde{\Theta}_f(\boldsymbol{\ell}'-\boldsymbol{\ell}'')\rangle \approx (2\pi)^2\delta_D(\boldsymbol{\ell}+\boldsymbol{\ell}')f(\ell'')f(|\boldsymbol{\ell}'-\boldsymbol{\ell}''|)$$

$$\times \int \frac{d\eta}{\eta^4}W^{\kappa}(\eta)\,[g(\eta)]^2\,B_{\delta p_{\hat{\mathbf{n}}}p_{\hat{\mathbf{n}}}}(\boldsymbol{\ell}/\eta, \boldsymbol{\ell}''/\eta, (\boldsymbol{\ell}'-\boldsymbol{\ell}'')/\eta) \quad (23)$$

Plugging this into eq. (20) gives

$$\langle\kappa(\boldsymbol{\ell})\Theta_f^2(\boldsymbol{\ell}')\rangle = (2\pi)^2\,\delta_D\left(\boldsymbol{\ell}+\boldsymbol{\ell}'\right)C^{\kappa\Theta_f^2}(\ell) \qquad (24)$$

with

$$C^{\kappa\Theta_f^2}(\ell) = \int \frac{d\eta}{\eta^2}W^{\kappa}(\eta)\,[g(\eta)]^2\,\mathcal{T}(k=\ell/\eta, \eta), \qquad (25)$$

and where we have defined

$$\mathcal{T}(k, \eta) \equiv \int \frac{d^2\mathbf{q}}{(2\pi)^2}\,f(q\eta)f(|\mathbf{k}+\mathbf{q}|\eta)B_{\delta p_{\hat{\mathbf{n}}}p_{\hat{\mathbf{n}}}}(\mathbf{k}, \mathbf{q}, -\mathbf{k}-\mathbf{q})\ .$$
$$(26)$$

This power spectrum in eq. (25) can be thought of as a Limber projection of the "power spectrum" $\mathcal{T}(k, \eta)$ which is an integral over all *planar* triangle configurations of the bispectrum $(\mathbf{k}, \mathbf{q}, -\mathbf{k}-\mathbf{q})$, with one of the sides of length k. It depends only on the norm of $\mathbf{k}$ by statistical isotropy and effectively collapses the three point information contained in $B_{\delta p_{\hat{\mathbf{n}}}p_{\hat{\mathbf{n}}}}$ (Cooray 2001b). We henceforth refer to eq. (26) as the *triangle power spectrum*.

3.2. *The hybrid bispectrum $B_{\delta p_{\hat{\mathbf{n}}}p_{\hat{\mathbf{n}}}}$*

In order to calculate the weak lensing kinetic SZ squared correlation, we must evaluate the hybrid bispectrum $B_{\delta p_{\hat{\mathbf{n}}}p_{\hat{\mathbf{n}}}}$ of the density and radial momentum component. Here we proceed by analogy with previous analytical studies of the kSZ power spectrum. The power spectrum of the radial momentum component is

$$\langle p_{\hat{\mathbf{n}}}(\mathbf{k})\,p_{\hat{\mathbf{n}}}(\mathbf{k}')\rangle = (2\pi)^3\,\delta_D(\mathbf{k}+\mathbf{k}')\,P_{p_{\hat{\mathbf{n}}}p_{\hat{\mathbf{n}}}}(k)\ . \quad (27)$$

Hu (2000) and then the joint numerical and analytical work of Ma & Fry (2000) suggested that the dominant contribution comes from non-linear densities coupling to linear bulk velocity flows. Furthermore, because of the cancellations that occur in the projection (Kaiser 1984), only the curl component of the projected momentum $\mathbf{p}$ - *i.e.* the component perpendicular to $\hat{\mathbf{n}}$ in the Fourier domain that we thus note $\mathbf{p}_{\perp}$- will contribute to the kSZ temperature fluctuation, so that

$$P_{p_{\hat{\mathbf{n}}}p_{\hat{\mathbf{n}}}}(k) \approx \frac{1}{2}P_{\mathbf{p}_{\perp}\mathbf{p}_{\perp}}(k) \approx \frac{1}{3}v_{\mathrm{rms}}^2 P_{\delta\delta}^{\mathrm{nl}}. \qquad (28)$$

where $v_{\rm rms}^2$ is the volume averaged velocity dispersion

$$v_{\rm rms}^2 = \int \frac{d^3\mathbf{k}}{(2\pi)^3} P_{vv}(k). \qquad (29)$$

We follow this analytical line of reasoning and make the following ansatz

$$B_{\delta p_{\hat{\mathbf{n}}} p_{\hat{\mathbf{n}}}} \approx \frac{1}{3} v_{\rm rms}^2 B_{\delta\delta\delta}^{\rm nl}, \qquad (30)$$

which presumes that the dominant contribution to the bispectrum in eq. (22) comes from large scale bulk velocity flows coupling to the three point function of the nonlinear density field. Note that at the 2 points level, analogous approximations can be motivated in a halo model context (Cooray & Sheth 2002; Sheth *et al.* 2003). Note however that it was also claimed, even if not clearly illustrated, that the curl component of the momentum induced by the vorticity in the non-linear velocity field itself might not be completely negligible (Zhang *et al.* 2003). If this were of some importance, then our evaluation would *underestimate* the signal of interest.

We are interested in the high-k, non-linear behavior of $\mathcal{T}(k)$, thus we need to evaluate the integral in eq. (26) with the fully nonlinear bispectrum of the density field. We use for this purpose the fitting function of Scoccimarro & Couchman (2001) for the bispectrum, *i.e.*

$$B_{\delta\delta\delta}^{\rm nl} = 2 F_2^{\rm eff}(\mathbf{k}_1, \mathbf{k}_2) P_{\delta\delta}^{\rm nl}(k_1) P_{\delta\delta}^{\rm nl}(k_2) + \text{cyclic} \qquad (31)$$

where

$$F_2^{\rm eff}(\mathbf{k}_1, \mathbf{k}_2) = \frac{5}{7} a(n_{\rm eff}, k_1) a(n_{\rm eff}, k_2)$$
$$+ \frac{1}{2} \frac{\mathbf{k}_1 \cdot \mathbf{k}_2}{k_1 k_2} \left(\frac{k_1}{k_2} + \frac{k_2}{k_1} \right) b(n_{\rm eff}, k_1) b(n_{\rm eff}, k_2)$$
$$+ \frac{2}{7} \left(\frac{\mathbf{k}_1 \cdot \mathbf{k}_2}{k_1 k_2} \right)^2 c(n_{\rm eff}, k_1) c(n_{\rm eff}, k_2). \qquad (32)$$

The fitting functions are given by

$$a(n_{\rm eff}, k) = \frac{1 + \sigma_8^{-0.2}(z) \sqrt{0.7 \, Q_3(n_{\rm eff})} \, (q/4)^{n_{\rm eff}+3.5}}{1 + (q/4)^{n_{\rm eff}+3.5}},$$

$$b(n_{\rm eff}, k) = \frac{1 + 0.4(n_{\rm eff}+3) q^{n_{\rm eff}+3}}{1 + q^{n_{\rm eff}+3.5}}, \qquad (33)$$

$$c(n_{\rm eff}, k) = \frac{1 + \left(\frac{4.5}{1.5 + (n_{\rm eff}+3)^4} \right) (2q)^{n_{\rm eff}+3}}{1 + (2q)^{n_{\rm eff}+3.5}},$$

where $n_{\rm eff}$ is the effective spectral index of the power spectrum,

$$n_{\rm eff}(k) \equiv \frac{d \ln P}{d \ln k}. \qquad (34)$$

The quantities q, Q, and $\sigma_8(z)$ are defined by

$$q \equiv \frac{k}{k_{\rm nl}} \quad \text{with} \quad \frac{k^3}{2\pi^2} P_{\delta\delta}^{\rm lin}(k_{\rm nl}, z) = 1, \qquad (35)$$

$$Q(n_{\rm eff}) = \frac{4 - 2^{n_{\rm eff}}}{1 + 2^{n_{\rm eff}+1}}, \qquad (36)$$

and

$$\sigma_8(z) = \int \frac{d^3\mathbf{k}}{(2\pi)^3} P_{\delta\delta}^{\rm lin}(k, z) W(kR) \qquad (37)$$

where $W(kR)$ is the usual Fourier transform of a top-hat of radius $R = 8 \, h^{-1}$ Mpc.

The functions $a(n_{\rm eff}, k)$, $b(n_{\rm eff}, k)$, and $c(n_{\rm eff}, k)$ in eq. (34) interpolate between the one loop perturbative expansion and highly non-linear regimes for general CDM cosmological models. It can be seen that for large scales, *i.e.* $k \ll k_{\rm nl}$, $a = b = c = 1$ and the tree level perturbation theory expression is recovered, whereas on small scales, *i.e.* $k \gg k_{\rm nl}$, $a = \sigma_8^{-0.2}(z) \sqrt{0.7 \, Q_3(n_{\rm eff})}$ and $b = c = 0$, so that the bispectrum becomes independent of triangle configuration.

3.3. *The Triangle Power Spectrum*

In this section we evaluate the triangle power spectrum for the simplest case where the filter functions are set to unity, $f(\ell) = 1$. In this case, a simple approximation exists in the high k limit that dramatically simplifies the computation and provides and intuitive understanding of the source and strength of the correlation. The full computation will be performed in for the purpose of computing the signal to noise ration in §6, one the appropriate filter is introduced.

The integral in eq. (26) will have three terms corresponding to the three permutations of the wave vectors in eq. (31)

$$\mathcal{T}(k) = \frac{1}{3} v_{\rm rms}^2 \left[\mathcal{T}_1(k) + \mathcal{T}_2(k) + \mathcal{T}_3(k) \right] \qquad (38)$$

where

$$\mathcal{T}_1(k) = 2P(k) \int \frac{d^2\mathbf{q}}{(2\pi)^2} F_2^{\rm eff}(\mathbf{k}, \mathbf{q}) P_{\delta\delta}^{nl}(q) \qquad (39)$$

$$\mathcal{T}_2(k) = 2P(k) \int \frac{d^2\mathbf{q}}{(2\pi)^2} F_2^{\rm eff}(\mathbf{k}, -\mathbf{k} - \mathbf{q}) P_{\delta\delta}^{nl}(|\mathbf{k} + \mathbf{q}|)$$

$$\mathcal{T}_3(k) = 2 \int \frac{d^2\mathbf{q}}{(2\pi)^2} F_2^{\rm eff}(\mathbf{q}, -\mathbf{k} - \mathbf{q}) P_{\delta\delta}^{nl}(q) P_{\delta\delta}^{nl}(|\mathbf{k} + \mathbf{q}|).$$

We first remark that $\mathcal{T}_2 = \mathcal{T}_1$ after a simple translation of the integration variable. Then, $\mathcal{T}_1$ can be evaluated exactly in polar coordinates because the angular integration factorizes out of the radial integration

$$\mathcal{T}_1(k) = \frac{P_{\delta\delta}^{\rm nl}(k)}{7\pi} \left[5 \, a(k) \int dq \, q \, a(q) P_{\delta\delta}^{\rm nl}(q) \right.$$
$$\left. + \quad c(k) \int dq \, q \, c(q) P_{\delta\delta}^{\rm nl}(q) \right], \quad (40)$$

where we abbreviate $a(n_{\rm eff}, k)$ as $a(k)$, and likewise for b and c. The remaining term $\mathcal{T}_3$, can be written

$$\mathcal{T}_3(k) = 2 \int \frac{d^2\mathbf{q}}{(2\pi)^2} \left[\frac{5}{7} a(q) a(|\mathbf{k} + \mathbf{q}|) \right.$$
$$- \frac{1}{2} b(q) b(|\mathbf{k} + \mathbf{q}|) \left(\frac{q}{|\mathbf{k} + \mathbf{q}|} + \frac{|\mathbf{k} + \mathbf{q}|}{q} \right) \left(\frac{q}{k} + \mu \right)$$
$$+ \left. \frac{2}{7} c(q) c(|\mathbf{k} + \mathbf{q}|) \left(\frac{q}{k} + \mu \right)^2 \right] P_{\delta\delta}^{\rm nl}(q) P_{\delta\delta}^{\rm nl}(|\mathbf{k} + \mathbf{q}|)$$
$$\qquad (41)$$

with $\mu \equiv \hat{\mathbf{k}} \cdot \hat{\mathbf{q}}$.

As mentioned previously, we are interested in the high-k, non-linear behavior of $\mathcal{T}(k)$ as the weak lensing kinetic

SZ squared correlation will only be significant on small angular scales. The dominant contributions to the integrals in eq. (40) will be for $\mathbf{q}$ near the peak of $P_{\delta\delta}^{nl}(q)$ where $a(q) \sim b(q) \sim c(q) \sim 1$. Thus in the high-$k$ limit the integrand is significant only for $q \ll k$, and we can drop terms of order $\mathcal{O}(q/k)$. A similar approximation has been used previously to calculate the mode coupling integrals for the kinetic SZ power spectrum (Hu 2000a; Ma & Fry 2001; Cooray 2001). In this approximation $\mathcal{T}_3 = \mathcal{T}_1$, and we get, introducing the dimensionless power spectra, $\Delta_{\mathcal{T}}^2$ and $\Delta_{\rm nl}^2$

$$\Delta_{\mathcal{T}}^2 = \frac{k^3}{2\pi^2}\mathcal{T} \quad \text{and} \quad \Delta_{\rm nl}^2 = \frac{k^3}{2\pi^2}P_{\delta\delta}^{\rm nl} , \qquad (42)$$

the following simple result

$$\Delta_{\mathcal{T}}^2(k,z) = \frac{1}{3}v_{\rm rms}^2(z)\,\Delta_{\rm nl}^2(k,z)\,E_3(k,z) \qquad (43)$$

where we defined the three point enhancement of the power spectrum

$$E_3(k,z) = \frac{6\pi}{7}\left[5\,a(k,z)\int d\ln q\,a(q,z)\frac{\Delta_{\rm nl}^2(q,z)}{q} \right.$$
$$\left. + \quad c(k,z)\int d\ln q\,c(q,z)\frac{\Delta_{\rm nl}^2(q,z)}{q} \right]. \quad (44)$$

Here the time dependence has been explicitly included in the functions above as a reminder. With these definitions, we obtain the final expression for the weak-lensing kSZ squared power spectrum

$$\frac{\ell^2}{2\pi}C_l^{\kappa\Theta^2} = \frac{\pi}{\ell}\int d\eta\,\eta\,W^\kappa(\eta)\,[g(\eta)]^2\,\Delta_{\mathcal{T}}^2(k = \ell/\eta, \eta) . \quad (45)$$

This intuitive result states that $C_l^{\kappa\Theta^2}$ is given by a 'Limber' projection of the triangle power spectrum, $\Delta_{\mathcal{T}}^2(k,z)$, which condenses information from all planar triangle configurations of the hybrid density-momentum bispectrum with side length k. The form of the triangle power spectrum in eq. (43) has as simple interpretation. It is similar to the kSZ power spectrum in eq. (28), in that it arises from density modulations of a large scale bulk flow. However, here we are dealing with three point modulations, which are *enhanced* by the non-linear coupling of small scale modes to large scale power. This mode coupling is encapsulated in the integrals over the power spectrum in $E_3(k,z)$. The dimensionless triangle power spectrum eq. (43) is shown in the right panel of fig. (3), along with the kSZ auto power spectrum eq. (28). Note that they have similar orders of magnitude.

4. UNDERSTANDING THE CORRELATION

Before calculating the signal to noise for the aforementioned cross correlations, we attempt to understand the degree to which the secondary anisotropies are correlated with weak lensing.

The strength of the angular correlation between any two random fields X and Y is quantified with the cross-correlation coefficient

$$\text{Corr}^{XY}(\ell) = \frac{C_\ell^{XY}}{\sqrt{C_\ell^{XX}C_\ell^{YY}}} \qquad (46)$$

As we are dealing with angular correlations of projected three dimensional fields (see eq. (7)), this cross-correlation coefficient will depend both on the extent to

which the window functions $W^X(\eta)$ and $W^Y(\eta)$ overlap, and the strength of of the cross power spectrum P_{XY} relative to the auto power spectra P_{XX} and P_{YY}.

If we change the integration variables from η to $k = \ell/\eta$, we can rewrite eq. (7) for the angular power spectrum, as an integral over wavenumber

$$\Delta_{XY}^2(\ell) = \int d\ln k\,H_\ell(k)\Delta_{XZ}^2(k, \eta = \ell/k) \qquad (47)$$

where

$$H_\ell^{XY}(k) \equiv \frac{\pi}{\ell}\left(\frac{\ell}{k}\right)^2 W^X(\ell/k)W^Y(\ell/k) \qquad (48)$$

With the above two equations, we can think of any cross correlation as a weighted integral of the cross power spectrum, Δ_{XY}^2, with the projection 'kernel' $H_\ell^{XY}(k)$. The kernels $H_\ell^{XX}(k)$ and $H_\ell^{YY}(k)$ indicate the scales probed by X and Y respectively, while the cross kernel $H_\ell^{XY}(k)$ indicates their degree of overlap.

The cross correlation coefficient for the kSZ²-weak lensing correlation is plotted in fig. 3. Computing this required the auto power spectrum of the kSZ temperature fluctuation squared $C_\ell^{\rm kSZ^2}$ (see §5 eq.(53)). The level of correlation is significant, approaching ~ 0.8 at the arc-min angular scales $\ell \gtrsim 3000$ in the damping tail, where the primary anisotropies are heavily attenuated.

The physical scales probed by these power spectra is illustrated in fig. 3, where we plot the projection kernels $H_\ell(k)$, for $C_\ell^{\kappa\kappa}$, $C_\ell^{\rm kSZ-kSZ}$, and $C_\ell^{\rm kSZ^2-\kappa}$, for $\ell = 1000$ and 10000. The 3-d power spectrum of the radial momentum $\Delta_{p_{\hat{n}}p_{\hat{n}}}^2$ and the triangle power spectrum $\Delta_{\mathcal{T}}^2$ are plotted in the right panel at $z = 0.5$. Note that the triangle power spectrum is of the same order of magnitude as the power spectrum responsible for the kSZ effect, $\Delta_{\mathcal{T}}^2 \sim \Delta_{p_{\hat{n}}p_{\hat{n}}}^2$.

The angular power spectrum is the projection of the power spectra on the right weighted by the kernels on the left (see eq.(47)), in this figure. The area under the $H_\ell(k)$ are normalized to unity. The sharp cutoff in the kernel for $C_\ell^{\rm kSZ-kSZ}$, occurs because we have assumed the universe is reionized abruptly at $\eta(z_{\rm rei} = 20)$ so that $W^{\rm kSZ}(\ell/k)$ drops to zero at small k.

We show the differential redshift contribution to each angular power spectrum as a function of redshift for $\ell = 5000$ in fig. 4, where we plot $\frac{1}{\Delta_{XY}^2(\ell)}\frac{d\Delta_{XY}^2(\ell)}{dz}$, for the auto and cross spectra. By definition, the area under each of these curves integrates to unity. While the kSZ auto power spectrum (dashed) has contributions from a high redshift tail, the bulk of the signal is skewed toward low z ~ 0.5, because of the growth of nonlinear structure. The overlap with the weak lensing (dotted) is thus apparent, explaining the large correlation coefficient found in fig. 2 (left).

5. DEPENDENCE ON POWER SPECTRUM NORMALIZATION

It is well known that the thermal SZ power spectrum exhibits a strong dependence on the power spectrum normalization parameter σ_8 (Komatsu & Seljak 2002; Seljak, Burwell, & Pen 2001; Zhang & Pen 2001), approximately scaling as the seventh power $C_\ell \propto \sigma_8^7$. This strong dependence suggests that the thermal SZ power spectrum might be an effective probe of σ_8, because even
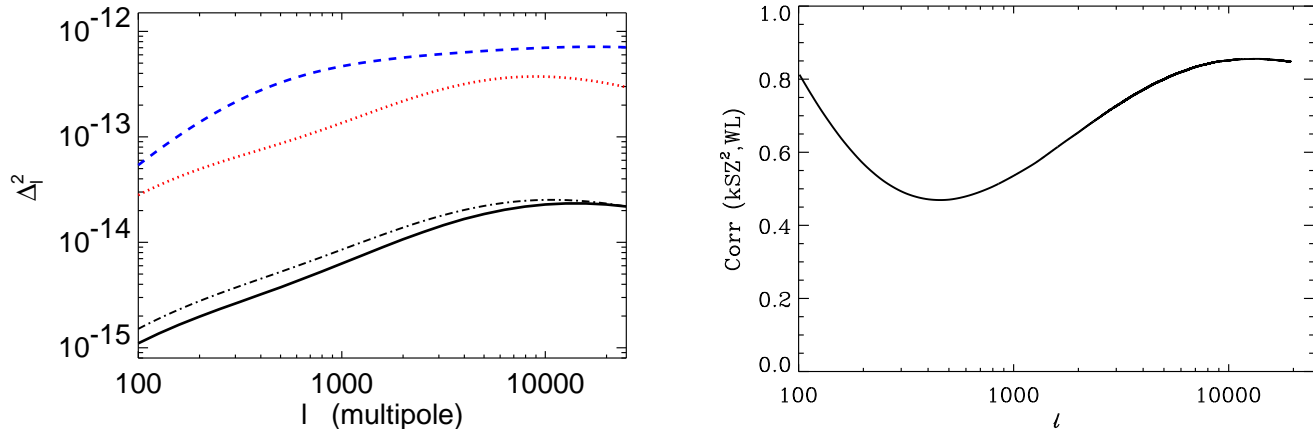
FIG. 2.— *Left:*Angular power spectra for kinetic SZ and kSZ^2-weak lensing cross correlation. Only dimensionless units are used. The blue solid line corresponds to the kSZ^2 auto power spectrum, while the red solid line corresponds to the WL auto power spectrum scaled down by a factor 10^9 for the sake of illustration. The kSZ^2-weak lensing angular cross power spectrum is shown by the solid (black) line. The dotted black line shows the result of using the approximation in eqn. (43) for the triangle power spectrum, which is good to $\sim 25\%$ for $\ell \gtrsim 3000$. The dashed (blue) line is the kinetic SZ auto power spectrum *Right:* Cross correlation coefficient for the kSZ^2-weak lensing correlation.
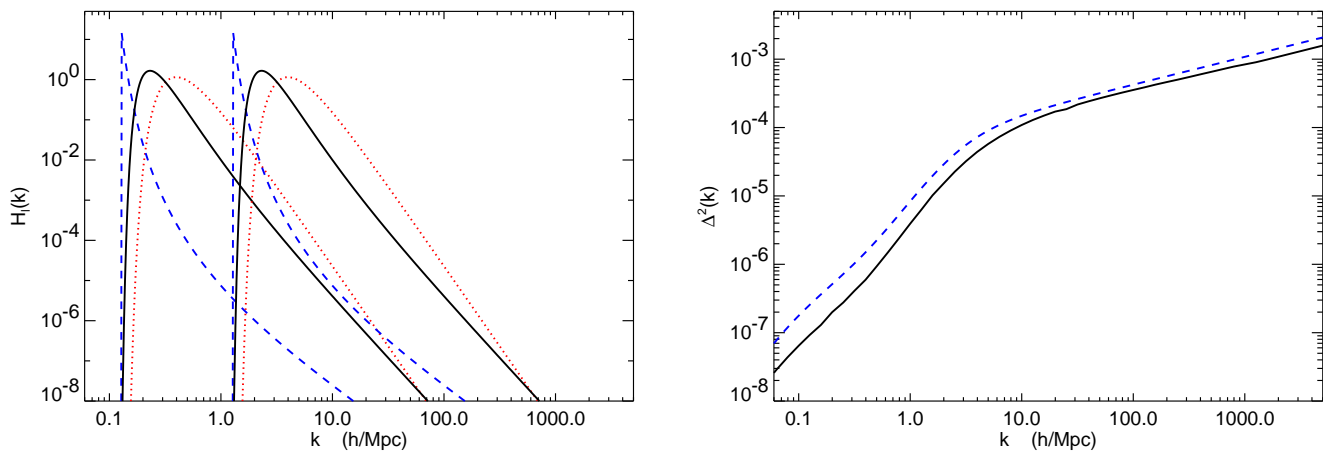

FIG. 3.— Projection Kernels for the weak lensing kinetic-SZ correlation: The left panel shows the projection kernels $H_\ell(k)$ for the the weak lensing auto correlation (dotted) $C_\ell^{\kappa\kappa}$, the kinetic-SZ auto correlation (dashed) $C_\ell^{\mathrm{kSZ-kSZ}}$, and the weak lensing-kinetic SZ squared cross-correlation (solid) $C_\ell^{\mathrm{kSZ}^2-\kappa}$. All kernels have been arbitrarily normalized to unit area. The leftmost set of curves indicate the range of wave-numbers contributing to the angular power spectrum at $\ell = 1000$; the rightmost set is for $\ell = 10000$. The right panel shows dimensionless 3-d power spectra of the radial momentum component (dashed) $\Delta_{p_{\hat{\mathbf{n}}}p_{\hat{\mathbf{n}}}}^2$ (eq. 28) and the triangular power spectrum (solid) $\Delta_{\mathcal{T}}^2$ (eq. 43). The triangle power spectrum is of the same order of magnitude as the power spectrum responsible for the kSZ effect, $\Delta_{\mathcal{T}}^2 \sim \Delta_{p_{\hat{\mathbf{n}}}p_{\hat{\mathbf{n}}}}^2$

if theoretical predictions are off by a factor of 2, this translates into less than 10% systematic error in σ_8.

We can determine the rough σ_8 dependence of the kSZ^2-weak lensing correlation from simple power counting if we recall that $C^{\mathrm{kSZ}^2-\kappa}{}_\ell \propto v_{\mathrm{rms}}^2 B_{\delta\delta\delta}$. The matter power spectrum scales as $P_{\delta\delta} \propto \sigma_8^{2-3}$ — two powers of σ_8 in the linear regime and three in the strongly nonlinear stable clustering regime. The large scale modes that give rise to the bulk flows in v_{rms}^2 are linear, so we expect $v_{\mathrm{rms}}^2 \propto P_{\delta\delta}^{\mathrm{lin}} \propto \sigma_8^2$. Finally, the bispectrum scales as $B_{\delta\delta\delta} \propto P_{\delta\delta}^2$, so putting everything together we expect the scaling $C_\ell^{\mathrm{kSZ}^2-\kappa} \propto \sigma_8^{6-8}$. Figure 5 illustrates the dependence of the cross power spectrum on σ_8. We find that

$C^{\mathrm{kSZ}^2-\kappa} \propto \sigma_8^7$ provides a good description of this scaling. This is similar to the strong seventh power scaling of the thermal SZ and suggests that the kSZ^2-weak lensing correlation might also serve as an effective probe of the power spectrum normalization and its redshift evolution.

6. PROSPECT FOR MEASUREMENT: SIGNAL TO NOISE ANALYSIS

In order to assess the detectability of the kSZ^2-weak lensing correlation we consider several current and future CMB experiment configurations and WL lensing survey specifications

On the CMB side, we consider the future PLANCK mission and the soon to be build ACT (Kosowsky 2003)
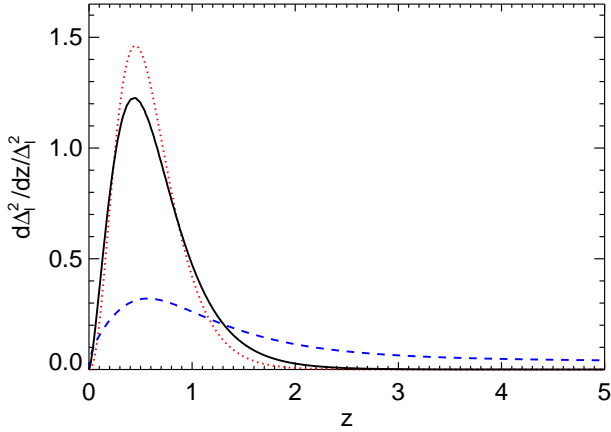
FIG. 4.— Differential redshift contributions to angular power spectra: Differential redshift contributions to the weak lensing auto correlation $\frac{\ell^2}{2\pi} C_\ell^{\kappa\kappa}$ (dotted), the kinetic-SZ auto correlation $\frac{\ell^2}{2\pi} C_\ell^{\Theta\Theta}$ (dashed), and the weak lensing-kinetic SZ squared cross-correlation $\frac{\ell^2}{2\pi} C_\ell^{\kappa\Theta^2}$ at $\ell = 5000$. All curves have been divided by the total power so that they integrate to unity.
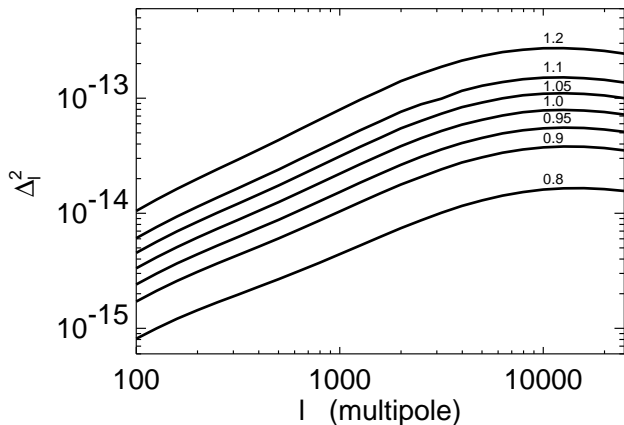

FIG. 5.— Dependence of the kSZ$^2 - \kappa$ cross correlation on σ_8. From top to bottom, the lines indicate σ_8=1.2, 1.1, 1.05, 1.0, 0.95, 0.9, and 0.8 as labeled in the figure.

telescope. Whereas the first one should offer a full sky survey ($f_{\rm sky} \simeq 0.85$ if one takes into account galactic contamination) the second one should conduct a smaller (100 square degree ($f_{\rm sky} \simeq 0.0025$)) but deeper survey. Both precise characteristics are summarized in table 1, where $\theta_{\rm fwhm}$ denotes the beam full width at half-maximum, σ_{pix} denotes the instrumental noise per θ^2 area pixels and "Area" denotes the observed sky area.

The subsequent expected errors are illustrated on fig. 1. Both have a frequency coverage appropriate for a proper tSZ "separation" so that we neglect this signal from now on (but the effects of residuals in § 6). On the lensing side, we consider 3 various surveys: the on-going Canada France Hawaii Telescope Legacy Survey (CFHTLS) [5],

[5] http://www.cfht.hawaii.edu/Science/CFHTLS

the future SNAP satellite [6] and the future ground based Large Synoptic Survey Telescope (LSST) [7]. Their key characteristics are summarized in table 2 and the expected uncertainties are illustrated in fig. 1 : z_0 denotes the redshift parameter of the source distribution of eq. (11), $n_{\rm gal}$ the mean density of galaxies, the surveyed area and the *single component* rms shear due to intrinsic ellipticity is σ_γ.

We define the optimal signal to noise per individual mode ℓ as

$$\left(\frac{S}{N}\right)_\ell^2 = \frac{\left(C_\ell^{XY}\right)^2}{{\rm Cov}\left[\left(C_\ell^{XY}\right)^2\right]} \ . \qquad (49)$$

To derive this formula, the assumption was made that all the relevant fields were Gaussian so that we end up naturally with the $S/(S+N)$ Wiener optimal weighting. Doing so, we follow *e.g.* Zaldarriaga (2000). We then approximate the covariance matrix by its diagonal, *i.e.* neglecting the correlation induced by the cut sky,

$$\left(f_{\rm sky}(2\ell+1)\right)^{-1}{\rm Cov}\left[\left(C_\ell^{XY}\right)^2\right] \ = $$
$$\left(C_\ell^X + N_\ell^X\right)\left(C_\ell^Y + N_\ell^Y\right) + \left(C_\ell^{XY}\right)^2 \ , \qquad (50)$$

where N_ℓ^{XX} denotes the evaluated instrumental noise contribution to the measured angular power spectrum of ℓ. For the weak lensing, it is simply the shot noise due to the intrinsic ellipticitie of the sources, *i.e.*

$$N_\ell^{WL} = \sigma_\gamma^2/n_{\rm gal} \ , \qquad (51)$$

whereas for the CMB, we include in the noise definition all the signal that can not be separated out using multi-frequency information and the conjunction of the noise and beam smearing give rise to (Knox 1995)

$$N_\ell^\Theta{}_{\rm instr} = \theta_{\rm fwhm}^2 \sigma_{\rm pix}^2/(4\pi) \ e^{\ell^2\theta_{\rm fwhm}^2/8\ln 2} \ . \qquad (52)$$

In the following subsections, we will consider two types of overlapping surveys. Either a small survey, like CFHTLS cross-correlated with either ACT or SPT, in which case the overlap area is limited by the sky coverage of say ACT, which is 100 square degrees, or a very large survey which uses PLANCK in conjunction with LSST or PANSTAR. In the latter case the total overlapping sky is limited by LSST, which is around 30,000 square degrees.

6.1. *Signal to noise for the kSZ^2-WL correlation*

TABLE 1
MAIN CHARACTERISTICS OF THE CMB EXPERIMENTS DISCUSSED.

	$\theta_{\rm fwhm}$	$\sigma_{\rm pix}$ [μK]	Area [deg.^{2}]
ACT/SPT[a]	1.7	2.	100.
PLANCK	5.	2.2	34000.

[a]SPT has in fact a wider but shallower survey but the correlation would thus be limited by lensing survey.
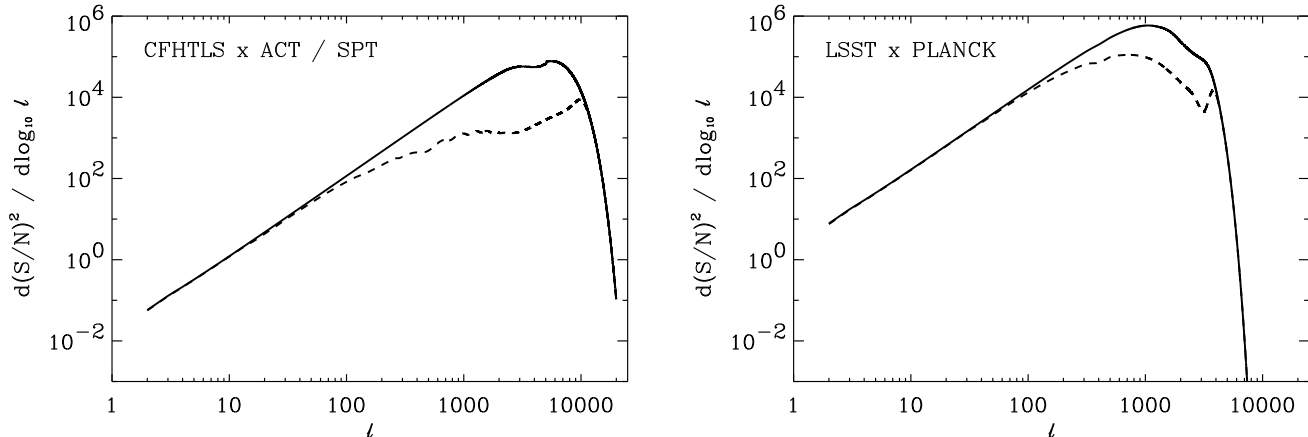
[6] http://snap.lbl.gov
[7] http://www.lssto.org

FIG. 6.— Signal to noise estimation for *logarithmic bins* in ℓ: The left panel assumes an ideal full sky measurement free of any instrumental noise. The middle panel illustrates the expectation for a 100 square degree of a CFHTLS like survey and ACT. The right panel assumes a LSST like 30 000 degree square degree and PLANCK. For each of those plot, the dashed line corresponds to a worst case scenario where the patchy reionisation contribution is 10 times higher (in temperature square units) than the kSZ one.

For this correlation, the dominant "noise" contribution that need to be considered at the relevant angular scales ($\sim 2'$, *i.e.* $\ell \simeq 5000$, see fig. 1) are the lensed primordial CMB, the potential patchy reionisation contribution and the instrumental noise. We neglect any residual tSZ signal and the subsequent correlation it would induced, we also neglect the "spurious" correlation due to lensing of the primordial CMB, although we discuss both of them in the next section. As is evident from fig. 1, the amplitude of spurious correlation with lensing of the CMB should be be more than 2 orders of magnitude weaker.

To evaluate both $C_\ell^{\mathrm{kSZ}^2\ \mathrm{kSZ}^2}$ and $N_\ell^{kSZ^2}$ involves one more approximation. We indeed have to evaluate the power spectrum of quantities squared in real space. To do so exactly would involve the computation of even higher order statistics, *e.g.* it would be a 8 point function for $C_\ell^{\mathrm{kSZ}^2\ \mathrm{kSZ}^2}$. To avoid such complications, we can reasonably consider those fields as being weakly non-gaussian, so that we can neglect this way their connected part, in particular the trispectrum of the squared field (Zaldarriaga 2000). With this hypothesis, the evolution of the power spectrum of those quantities translates in a convolution in harmonic space that can be easily performed numerically :

$$C^{X^2}(\boldsymbol{\ell}) \simeq 2 \int \frac{d^2\boldsymbol{\ell}'}{(2\pi)^2} C^X(\boldsymbol{\ell}')\ C^X(\boldsymbol{\ell} - \boldsymbol{\ell}') \qquad (53)$$

TABLE 2
MAIN CHARACTERISTICS OF THE WEAK-LENSING SURVEYS DISCUSSED.

	$z0$	n_{gal} [gal.arcmin^{-2}]	Area [deg.^{2}]	σ_γ
$CFHTLS$	0.5	20.	170.	0.31
$SNAP$	0.9	100.	300.	0.23
$LSST$	0.75	75.	30000.	0.16

$$\simeq \int \frac{\ell' d\boldsymbol{\ell}'}{\pi} C^X(\ell')\ C^X(|\boldsymbol{\ell} - \boldsymbol{\ell}'|)$$

We evaluate the convolution above numerically using the full power spectrum of primary plus secondary anisotropies. With this, we can compute all the required quantities in eq. (49).

Before computing the theoretical prospects for the experimental configurations we consider, it is crucial to realize that before squaring the Θ field, an appropriate filtering is necessary. Indeed, as visible *e.g.* in eq. (53), this squaring will introduce violent mode-coupling, so that any signal that has a strong power outside the range where the kSZ signal dominates will pollute the quadratic field. It would be possible using our theoretical knowledge of the shape of the cross-correlation power spectrum $C_\ell^{\kappa\Theta_{\mathrm{kSZ}}^2}$, although a bit cumbersome, to compute an optimal filter for our statistics (Hu 2002). Instead we take a reasonable short cut. Given the fact that both C_ℓ^κ and $C_\ell^{\kappa\Theta_{\mathrm{kSZ}}^2}$ are nearly flat in the range where the kSZ dominates, we will consider indeed as the filter for our cross-correlation signal the one that maximizes the kSZ signal alone. This last one can be easily derived if we assume that the projected kSZ signal is weakly non-Gaussian. It is indeed given by the usual Wiener filter (Bouchet & Gispert 1999; Tegmark & Efstathiou 1996)

$$f_\ell = \frac{C_\ell^{\mathrm{kSZ}}}{C_\ell^{\mathrm{Noise}} + C_\ell^{\mathrm{kSZ}}} \qquad (54)$$

where C_ℓ^{Noise} includes the instrumental noise but also all the other astrophysical component different from the kSZ itself. Note that this filter is similar to the one derived in a more general manner by Hu (2002) and employed by Cooray (2001a).

The results are illustrated in fig. 6 where we plot the contribution to the square of signal to noise per log ℓ. We consider two situations: i/ the dashed line corresponds to a situation where the patchy reionisation is present and strong, *i.e.* we consider the higher amplitude model of (Santos *et al.* 2003), where the patchy reionisation power spectrum amplitude is about 10 times higher than

the kSZ one in the same angular range (see fig. 1) ii/ the solid line corresponds to a scenario where the patchy reionisation component is completely negligible.

Obviously, this signal should be easily detectable using a CFHTLS-ACT configuration. The overall signal to noise ratio reaches 225 if the patchy reionization is negligible, 47 otherwise. The signal to noise per individual ℓ reaches 1.8. For the PLANCK-LSST configuration, the signal reaches 978 without no patchy reionization and 473 otherwise. However, as we discuss in the next section, this kSZ signal will probably be heavily contaminated by thermal SZ residuals.

6.2. *Spurious Correlations*

The primary limitation to detecting the kSZ^2-weak lensing correlation will certainly come from spurious sources of correlation. Possible sources of anisotropy other than kSZ that the weak lensing may correlate with are tSZ residuals from imperfect frequency cleaning, weak lensing of the primordial CMB, and point sources. We discuss each in turn.

The dominant spurious correlation will probably be that due to the residual tSZ after frequency cleaning. Cooray *et al.* (2000) estimated that for PLANCK, the power spectrum of the residual for $600 < \ell < 2500$ should be around 0.14 times the initial tSZ power spectrum, *i.e.* around 5 times the kSZ for our model. Since the correlation coefficient around WL and tSZ is expected to be around 0.6 (Seljak, Burwell, & Pen 2001), the correlated component between tSZ residuals and WL will probably be more significant than the correlation with kSZ. For ACT/SPT telescope, the frequency coverage will allow for frequency cleaning as good as if not better than PLANCK, while the higher resolution provides improved sensitivity at the scales where the tSZ dominates, $\ell > 2000$ (see fig. 1), so frequency cleaning should be drastically improved at those scales. Further consideration of this issue is required, but we defer this to a future work.

Another source of spurious correlation should be the correlation induced between the lensed primordial CMB and the WL. Here again, this effect might be important for PLANCK as visible in fig. 1 but should be negligible for ACT/SPT since in the range of interest, the lensed contribution of the CMB is around 2 orders of magnitude weaker than the kSZ one. In addition, any attempt to cross correlate CMB lensing with cosmic shear (Hu 2002) will need to consider the kSZ^2-weak lensing signal as a source of spurious correlation, since this signal will begin to dominate for $\ell \sim 3000$ near the damping tail.

Finally, there is the possibility of spurious correlation with point sources. At the frequencies of interest, this is primarily dust emission from sub-mm galaxies. This population of objects will probably correlate with the weak lensing signal but the strength of that correlation is rather uncertain.

Finally, we note that the kSZ^2-weak lensing correlation has a specific signature that may alleviate some of the problems with spurious correlation and could provide a mechanism to isolate the kSZ signal. Specifically, the kSZ effect does not correlate with weak lensing at the 2 point level, whereas tSZ residuals or dusty sub-mm galaxies will. It may be possible to exploit this fact, and remove the part of the anisotropy that correlates with weak lensing at the two point level. This would effectively "lensing clean" the temperature map so that the residuals would be dominated by the kSZ. Realistic simulations are certainly required to precisely evaluate the potential of this technique, but this is outside the scope of this paper.

7. CONCLUSION

We have evaluated the prospects for upcoming experiments to measure the correlation between arc-minute scale secondary anisotropies of the CMB and cosmic shear, after tSZ has been removed by frequency cleaning. In particular, we evaluated the signal to noise ratio for the kSZ^2-weak lensing correlation.

The two point correlation of kSZ with and density tracer is negligible because of the isotropy of the velocity field; however, we found that a strong 3-point correlation exists. A collapsed three point statistic was introduced to measure the three point signal, which is the angular cross power spectrum between weak lensing and the square of the filtered temperature. While residual thermal SZ will limit the detectability of this correlation for PLANCK-LSST, it should be easily detectable by cross correlation ACT/SPT with the CFHTLS/SNAP at $\ell \sim 5000$ where the signal to noise ratio per ℓ reaches 1.8. In principle, a full analysis of the cross bispectrum $B^{\kappa\Theta\Theta}_{\ell_1\ell_2\ell_3}$ could yield a higher signal to noise — a calculation we defer to a future paper.

The kSZ^2-weak lensing correlation probes three point correlations between the underlying dark matter and the the *momentum* of the ionized baryons in dense regions, providing the only known probe into this physics. We presumed that these higher order correlations, or more precisely the hybrid bispectrum $B_{\delta p_{\hat{n}} p_{\hat{n}}}$, arose from three point density modulations of large scale coherent motions. The situation is surely more complicated and this approximation must be compared to hydrodynamic numerical simulations. Nevertheless, measurement of kSZ^2-weak lensing correlation will provide valuable insights into the physics of energy injection, the bias and ionization fraction of baryons in the densest environments, and information on the nonlinear mode coupling between dark matter and baryons. We also considered the dependence of correlation signal on the power spectrum normalization parameter σ_8 and determined the approximate scaling $C_\ell \propto \sigma_8^7$ similar to the scaling of the tSZ power spectrum.

Despite the interest in detection of the kSZ^2-weak lensing correlation, a null detection could prove equally interesting. The contribution of patchy reionization to arc-minute scale anisotropy in the CMB is a contentious issue, with different reionization models and histories predicting signal amplitudes differing by several orders of magnitude (Aghanim, Desert, Puget, & Gispert 1996; Gruzinov & Hu 1998; Knox, Scoccimarro, & Dodelson 1998; Santos *et al.* 2003; Valageas *et al.* 2001). The lack of a correlation in the presence of significant arc-minute scale anisotropy would indicate that this anisotropy was generated at high redshift, rather than in the low redshift universe probed by weak gravitational lensing. This last point is especially important when one considers the similarity in shape between the power spectrum of patchy reionization and that of kinetic SZ (see fig. 1).

In addition, we note that many of the calculations in this paper can be directly applied to correlations with galaxies rather than weak lensing as the tracer of density field, given a suitable model for the bias of galaxies in the nonlinear regime, as provided by, *e.g.* the recently popular halo model (Cooray & Sheth 2002; Sheth *et al.* 2003). The weak lensing window function $W^\kappa(\eta)$, would simply be replaced with a suitable window function for the galaxies. As the noise in the correlation measurement is dominated by the CMB, the signal to noise per square degree should not change significantly. However, because large area galaxy surveys already exist, the correlations we discussed might be measured with galaxies first, as was the case recently for the ISW effect (Afshordi *et al.* 2003; Boughn & Crittenden 2003; Fosalba & E. Gatzanaga 2003; Fosalba *et al.* 2003; Nolta *et al.* 2003; Scranton *et al.* 2003). The kSZ^2-galaxy correlation would probe three point correlations between the density of galaxies and the momentum of ionized baryons in clusters, providing valuable information about galaxy formation.

With such a high signal to noise ratio, it is conceivable that radial information might also be extracted from the cross-correlation. If photometric redshifts of background source galaxies were available, one could attempt to deproject the cross-correlation tomographically. Similarly, if galaxies were correlated with kSZ^2 rather than weak lensing, galaxy photo-z's could be use to extract this radial information. This has been discussed in the context of galaxy-tSZ cross correlation by Zhang & Pen (2001). Studying the cross-correlation as a function of redshift would yield information on the redshift evolution of the dynamical state of baryons in dense environments.

In conclusion, our study predicts that coming arcminute scale measurements of the secondary anisotropies of the CMB should will correlate strongly with local tracers of the density field, like weak gravitational lensing or galaxies from large scale structure surveys. The total signal to noise ratio for the kSZ^2-weak lensing correlation is greater than 220 for ACT/SPT correlated with CFHTLS/SNAP, which will be easily detectable. We believe that this signal along with the other cross-correlations with cosmic shear studied by Seljak, Burwell, & Pen (2001) and Hu (2002), provide a significant incentive for upcoming CMB experiments and lensing surveys to image the same regions of sky.

REFERENCES

Aghanim, N., Desert, F. X., Puget, J. L., & Gispert, R. 1996, A&A, 311, 1
Afshordi, N. *et al.* 2003, astro-ph/0308260
Bean, R., Melchiorri, A., & Silk, J., accepted in Phys. Rev. D, astro-ph/0306357
Bouchet, F. R. & Gispert, R. 1999, New Astronomy, 4, 443
Bond, J. R. *et al.* , Phys. Rev. D, astro-ph/0205386
S.P. Boughn, R.G Crittenden astro-ph/0305001
Buchalter, A., Kamionkowski, M., & Jaffe, A. H. 2000, ApJ, 530, 36
Castro, P. G. 2003, Phys. Rev. D, 67, 123001
Cooray, A. 2001, Phys. Rev. D, 64, 43516
Cooray, A. 2001, Phys. Rev. D, 64, 63514
Cooray, A. & Hu, W. 2000, ApJ, 534, 533
Cooray, A., Hu, W., & Tegmark, M. 2000, ApJ, 540, 1
Cooray, A., Sheth, R., astro-ph/0206508, and references therein
Cooray, A. & Melchiorri, A. 2002, Phys. Rev. D, 66, 83001
da Silva, A. C., Barbosa, D., Liddle, A. R., & Thomas, P. A. 2001, MNRAS, 326, 155
Dawson, K. S., Holzapfel, W. L., Carlstrom, J. E., Joy, M., & LaRoque, S. J. 2002, American Astronomical Society Meeting, 201,
Dodelson, S. & Jubas, J. M. 1995, ApJ, 439, 503
Doré, O. & Hennawi, J. F., Seljak, U., & Spergel, D. N. 2003, in preparation
P. Fosalba & E. Gatzanaga, astro-ph/0305468
P. Fosalba & E. Gatzanaga, astro-ph/0307249
Goldberg, D. M. & Spergel, D. N. 1999, Phys. Rev. D, 59, 103002
Gnedin, N. Y. & Jaffe, A. H. 2001, ApJ, 551, 3
Griffiths, L. M., Barbosa, D., & Liddle, A. R. 1999, MNRAS, 308, 854
Griffiths, L. M., Kunz, M., & Silk, J. 2003, MNRAS, 339, 680
Gruzinov, A. & Hu, W. 1998, ApJ, 508, 435
Hamilton,A.J.S., Matthews, A., Kumar, P., Lu, E. 1991, ApJ, 374, L1
Holder, G. P. 2002, ApJ, 580, 36
Hu, W. & White, M. 1996, A&A, 315, 33
Hu, W. 2000, ApJ, 529, 12
Hu, W. 2000, Phys. Rev. D, 62, 043007
Hu, W. 2002, Phys. Rev. D, 65, 23003
Jaffe, A. H. & Kamionkowski, M. 1998, Phys. Rev. D, 58, 43001

Knox, L., Scoccimarro, R., & Dodelson, S. 1998, Phys. Rev. Lett., 81, 2004
Komatsu, E. & Seljak, U. 2002, MNRAS, 336, 1256
A. Kosowsky, astro-ph/0301131
Kaiser, N. 1984, ApJ, 282, 374
Kaiser, N. 1992, ApJ, 388, 272
Knox, L. 1995, Phys. Rev. D, 52, 4307
Ma, C.P. 1998, ApJ,508,L5
Ma, C. & Fry, J. N. 2000, ApJ, 531, L87
Ma, C. & Fry, J. N. 2002, Phys. Rev. Lett.88, 211301
Mason, B. S. *et al.* 2003, ApJ, 591,540
Monin, A. S. & Yaglom, A. M. 1971, Statistical Fluid Mechanics, Vol. 2 (Cambridge: MIT Press)
M.R. Nolta *et al.* astro-ph/0305097
Oh, P., Cooray, A., Kamionkowski, M. *et al.* , astro-ph/0303007
Ostriker, J. P. & Vishniac, E. T. 1986, ApJ, 306, L51
Peacock, J. A. & Dodds, S. J. 1996, MNRAS, 280, L19
Peiris H. V., Spergel D. N., 2000, ApJ, 540, 605
Refregier, A. & Teyssier, Phys. Rev. D, 2002, 66, 043002
Rees M.J., Sciama D.W., 1968, Nature, 217, 511
Sachs, R. K. & Wolfe, A. M. 1967, ApJ, 147, 73
Santos, M. astro-ph/0305471
Scannapieco, E. 2000, ApJ, 540, 20
Scoccimarro, R. & Couchman, H. M. P. 2001, MNRAS, 325, 1312
Scranton, R. *et al.* 2003, astro-ph/0307335
Seljak, U. & Zaldarriaga, M. 1999, Phys. Rev. D, 60, 43504
Seljak, U., Burwell, J., & Pen, U. 2001, Phys. Rev. D, 63, 63001
Sheth, R. K. , Zehavi, I. & Diaferio, A. 2003, submitted to MNRAS
Smith, R.E., Peacock, J.A., Jenkins, A., White, S.D.M, Frenk,C.S.,Pearce,F.R., Thomas, P.A.,Efstathiou, G., Couchman, H.M.P
Spergel, D. N. & Goldberg, D. M. 1999, Phys. Rev. D, 59, 103001
Spergel, D. *et al.* , submitted to ApJ, astro-ph/0302209
Springel, V., White, M., & Hernquist, L. 2001, ApJ, 549, 681
Sunyaev,R.A. & Zel'dovich, Ya. B., 1980, MNRAS, 190, 413
Takada, M. & Sugiyama, N. 2002, ApJ, 569, 8
Tegmark, M. & Efstathiaga, G. 1996, MNRAS, 281, 1297
Tegmark, M., Eisenstein, D. J., Hu, W., de Oliveira-Costa, A., 2000, ApJ, 530, 133
Valageas, P., Balbi, A., & Silk, J. 2001, A&A367,1
Van Waerbeke, L. & Mellier, Y., astro-ph/0305089

Vishniac, E. T. 1987, ApJ, 322, 597

Verde, L. & Spergel, D. N. 2002, Phys. Rev. D, 65, 3007

White, M., Carlstrom, J. E., Dragovan, M., & Holzapfel, W. L. 1999, ApJ, 514, 12

Zaldarriaga, M. 2000, Phys. Rev. D, 62, 63510

Zhang, P. & Pen, U. L 2001, ApJ, 549, 18

Zhang, P. , Pen, U. L. & Trac, H., `astro-ph/0304534`